AGU PUBLICATIONS

JGR

Journal of Geophysical Research: Atmospheres

RESEARCH ARTICLE
10.1002/2016JD026415

Key Points:
- Updating the SOA module of the STOCHEM-CRI chemistry scheme by incorporating a detailed oxidation mechanism of β-caryophyllene
- The addition of sesquiterpenes increases the SOA global burden and production rate by 0.11 Tg and 12.9 Tg/yr, respectively
- Globally, up to 1.2 μg/m^3 sesquiterpene-derived SOA were seen over central Africa and South America

Supporting Information:
- Supporting Information S1
- Supporting Information S2

Correspondence to:
D. E. Shallcross,
d.e.shallcross@bristol.ac.uk

Citation:
Khan, M. A. H., M. E. Jenkin, A. Foulds, R. G. Derwent, C. J. Percival, and D. E. Shallcross (2017), A modeling study of secondary organic aerosol formation from sesquiterpenes using the STOCHEM global chemistry and transport model, *J. Geophys. Res. Atmos.*, *122*, doi:10.1002/2016JD026415.

Received 21 DEC 2016
Accepted 28 MAR 2017
Accepted article online 29 MAR 2017

A modeling study of secondary organic aerosol formation from sesquiterpenes using the STOCHEM global chemistry and transport model

M. A. H. Khan[1], M. E. Jenkin[1,2], A. Foulds[1], R. G. Derwent[3], C. J. Percival[4,5], and D. E. Shallcross[1]

[1]Atmospheric Chemistry Research Group, School of Chemistry, University of Bristol, Bristol, UK, [2]Atmospheric Chemistry Services, Okehampton, UK, [3]rdscientific, Newbury, UK, [4]Centre for Atmospheric Science, School of Earth, Atmospheric and Environmental Science, University of Manchester, Manchester, UK, [5]Now at NASA Jet Propulsion Laboratory, Pasadena, California, USA

Abstract Sesquiterpenes are one of the precursors of secondary organic aerosol (SOA) which can be an important global sources of organic aerosol (OA). Updating the chemistry scheme in the global chemistry transport model by incorporating an oxidation mechanism for β-caryophyllene (representing all sesquiterpenes), adding global sesquiterpene emissions of 29 Tg/yr, and revising global monoterpene emissions up to 162 Tg/yr [*Guenther et al.*, 2012] led to an increase of SOA burden by 95% and SOA production rate by 106% relative to the base case described in *Utembe et al.* [2011]. Including the emissions of sesquiterpenes resulted in increase of SOA burden of 0.11 Tg and SOA production rate of 12.9 Tg/yr relative to the base case. The highest concentrations of sesquiterpene-derived SOA (by up to 1.2 μg/m^3) were found over central Africa and South America, the regions having high levels of biogenic emissions with significant biomass burning. In the updated model simulation, the multigeneration oxidation products from sesquiterpenes and monoterpenes transported above the boundary layer and condensed to the aerosol phase at higher altitude led to an increase of OA by up to 30% over the tropics and northern midlatitude to higher altitude. The model evaluation showed an underestimation of model OA mostly for the campaigns dominated by regional anthropogenic pollution. The increase of SOA production from sesquiterpenes reduced the discrepancies between modeled and observed OA concentrations over the remote and rural areas. The increase of SOA concentrations by up to 200% from preindustrial to present scenarios was found over the tropical oceans.

1. Introduction

Organic aerosols (OA) have a large impact on air quality, biogeochemistry, and the climate through interactions with reactive trace gases, water vapor, clouds, precipitation, and radiation [*Intergovernmental Panel on Climate Change (IPCC)*, 2013]. They can affect biogeochemistry through either their deposition of nutrients on land or ocean or by changing climate [*Mahowald et al.*, 2011]. They can influence climate by changing the Earth's energy budget by scattering and absorbing the radiation or acting as cloud condensation nuclei. However, they represent one of the largest uncertainties in climate science, being for the most part a climate cooling species [*IPCC*, 2013].

OA can originate as either a primary organic aerosol (POA) or a secondary organic aerosol (SOA). POAs are emitted into the atmosphere from biomass burning, fossil fuel and biofuel use, and sea spray. SOA is defined as products of gas-phase oxidation or as emitted volatile organic compounds (VOC) from biogenic or anthropogenic sources, such as vegetation and combustion emissions (e.g., aldehydes like nonanal and polycyclic aromatic hydrocarbons like pyrene and naphthalene), which have partitioned from the gas to the aerosol phase [*Kroll and Seinfeld*, 2008; *Hallquist et al.*, 2009]. However, SOA remains the least understood aerosol component because organics (gas and particles) comprise of a mixture of an extremely large number of organic compounds [*Goldstein and Galbally*, 2007], with each compound further undergoing atmospheric chemical reactions to produce a range of oxidized products [*Hallquist et al.*, 2009]. Based on the mass balance of volatile organic carbon or on scaling of the sulphate budget, the global sources of SOA are estimated to between 120 and 1820 Tg/yr [*Goldstein and Galbally*, 2007; *Hallquist et al.*, 2009]. Recently, *Tsigaridis et al.* [2014] estimated SOA annual production rates ranging

from 13 to 119 Tg/yr by using 31 global chemistry transport and general circulation models. A number of studies suggested important pathways of SOA production from volatile organic precursors such as isoprene and monoterpenes [*Kroll et al.*, 2006; *Paulot et al.*, 2009; *Carlton et al.*, 2009; *Utembe et al.*, 2011] or aromatic compounds [*Hildebrandt et al.*, 2009; *Ng et al.*, 2007; *Henze et al.*, 2008; *Sato et al.*, 2012; *Li et al.*, 2016], heterogeneous uptake of glyoxal and methylglyoxal [*Kroll et al.*, 2005; *Ervens et al.*, 2008, 2011; *Carlton et al.*, 2007; *Volkamer et al.*, 2007, 2009; *Fu et al.*, 2008; *Lin et al.*, 2012], and oxidation of low vapor pressure intermediate-volatility and semivolatile organic compounds [*Robinson et al.*, 2007; *Jimenez et al.*, 2009; *Pye and Seinfeld*, 2010; *Jathar et al.*, 2011; *Hodzic et al.*, 2016]. The underestimation of model SOA compared with measured SOA [*Volkamer et al.*, 2006; *Utembe et al.*, 2011] suggested missing SOA precursors or underestimated atmospheric processing of organics in the model. Thus, the representation in global chemistry transport models of the myriad of chemical processes involved in SOA formation has proven to be a challenging task.

Previous studies have shown that the oxidation of biogenic VOCs makes a major contribution to global SOA formation [e.g., *Tsigaridis et al.*, 2006; *Henze et al.*, 2008; *Utembe et al.*, 2011]. Although isoprene and monoterpenes are generally emitted more abundantly, sesquiterpenes have received increasing interest in recent years owing to the exceptionally high reactivity of some species, particularly toward ozone [*Atkinson and Arey*, 2003; *Jardine et al.*, 2011; *Richters et al.*, 2015], and their generally high propensity to form SOA upon oxidation [*Hoffmann et al.*, 1997; *Jaoui et al.*, 2004; *Lee et al.*, 2006a, 2006b; *Ng et al.*, 2007]. The β-caryophyllene has received particular attention, being one of the most reactive and abundant sesquiterpenes, and SOA yields have been reported in a number of ozonolysis and photo-oxidation studies [*Hoffmann et al.*, 1997; *Griffin et al.*, 1999; *Jaoui et al.*, 2003; *Lee et al.*, 2006a, 2006b; *Winterhalter et al.*, 2009; *Alfarra et al.*, 2012; Tasoglou and Pandis, 2015]. As a result, its atmospheric degradation has been the subject of a number of experimental and theoretical mechanistic appraisals [*Calogirou et al.*, 1997; *Jaoui et al.*, 2003; *Lee et al.*, 2006b; *Kanawati et al.*, 2008; *Winterhalter et al.*, 2009; *Nguyen et al.*, 2009; *Zhao et al.*, 2010; *Li et al.*, 2011; *Chan et al.*, 2011; *Jenkin et al.*, 2012], and several established oxidation products have been used in tracer studies to show that β-caryophyllene-derived SOA makes potentially important contributions to ambient fine particulate matter at a number of locations [*Jaoui et al.*, 2007; *Kleindienst et al.*, 2007; *Parshintsev et al.*, 2008].

Most atmospheric modeling studies, in which the oxidation of β-caryophyllene (and/or other sesquiterpenes) has been treated, have used highly simplified or parameterized representations of the chemistry [*Lane et al.*, 2008; *Sakulyanontvittaya et al.*, 2008; *Carlton et al.*, 2010; *Zhang and Ying*, 2011], with SOA formation represented by assigning empirically derived yields and partitioning coefficients to notional products, based on the results of chamber studies. While such approaches are practical and economical, the gas-phase formation and evolution of low-volatility products of VOC oxidation are known to be sensitive to the prevailing atmospheric conditions, and it is ideally necessary to understand and represent the competitive reactions involved over several generations of oxidation, if SOA formation, and its dependence on conditions, is to be represented rigorously [Kroll and Seinfeld, 2008; *Hallquist et al.*, 2009]. More explicit representations of β-caryophyllene oxidation have therefore been considered in some recent studies [*Li et al.*, 2015], based on the highly detailed chemistry in the Master Chemical Mechanism (MCM v3.2).

Utembe et al. [2011] have previously used the STOCHEM-Common Representative Intermediates (STOCHEM-CRI) 3-D global chemistry transport model to demonstrate that condensable species formed over several generations of VOC oxidation contribute to SOA formation, with important contributions from second- and third-generation oxidation products of monoterpenes in the upper troposphere. The simulated vertical distribution of OA agreed well with observations, but the absolute mass loadings were consistently underestimated by a factor of about 5. *Utembe et al.* [2011] discussed a number of possible reasons for this discrepancy, which included missing contributions from unrepresented SOA precursors, such as sesquiterpenes. In this paper, we describe an update to the SOA module of the CRI v2-R5 mechanism used by *Utembe et al.* [2011], in which a detailed oxidation mechanism of β-caryophyllene (representing all sesquiterpenes), traceable to MCM v3.2 [*Jenkin et al.*, 2012], has been implemented. The global formation and distribution of OA are simulated, highlighting the contributions of SOA from sesquiterpenes using the updated STOCHEM-CRI. We show a comparison between model results and a wide range of measurements of SOA from flight data sets and individual field measurements.

2. Model Description

A global three-dimensional Chemistry Transport Model, STOCHEM used in this work was developed at the UK Meteorological Office. In STOCHEM, the troposphere is divided into 50,000 constant mass air parcels, which are advected every 3 h by using a Lagrangian approach allowing the chemistry and transport processes to be uncoupled [*Stevenson et al.*, 1998]. STOCHEM is an "off-line" model with the transport and radiation codes driven by archived meteorological data from the UK Meteorological Office Unified Model, which operates at a grid resolution of 1.25° longitude × 0.83° latitude × 12 unevenly spaced vertical levels, with an upper boundary up to 100 hPa [*Johns et al.*, 1997]. STOCHEM is a computationally efficient model which allows the implementation of a detailed chemistry mechanism (CRI v2-R5) for the study of ozone, odd-H, and related species within the troposphere.

The gas-phase chemical mechanisms used in this study was developed by *Jenkin et al.* [2008] and *Watson et al.* [2008]. *Jenkin et al.* [2008] produced the first variant known as the Common Representative Intermediates mechanism version 2 (CRI v2). The CRI v2 was developed on a compound-by-compound basis by using 5 day box model simulations with the performance of the chemistry for each compound being compared and optimized with the MCM v3.1 with ozone production being the primary criterion. CRI v2 reduces the number of species and reactions in the MCM v3.1 by around 90% (to 434 species and 1183 reactions), while still describing the degradation of methane and 115 nonmethane VOCs [*Jenkin et al.*, 2008]. By considering a series of emission lumping options for anthropogenic VOCs, a set of five further reduced CRI v2 mechanisms were developed by *Watson et al.* [2008], with the most reduced CRI v2-R5 scheme applied here having 220 species and 609 reactions for the degradation of 22 emitted nonmethane VOC compounds [*Utembe et al.*, 2009].

The SOA code applied in the present study has been described in detail previously [*Utembe et al.*, 2009, 2011]. The formation of SOA is represented in terms of the equilibrium partitioning of the oxygenated products between the gas and condensed organic phases according to the method of *Pankow* [1994]. *Utembe et al.* [2009, 2011] represented phase partitioning for a total of 14 CRI v2-R5 species, comprising 10 monoterpene-derived biogenic species, one isoprene-derived biogenic species, and three aromatic hydrocarbon-derived species. Each species acts as a surrogate, used to represent a set of species in the reference MCM v3.1 code, which were initially assigned partitioning coefficients based on those for the closest analogous species in MCM v3.1. The values of the partitioning coefficients were then scaled to optimize agreement with the results of MCM v3.1 reference simulations for a set of 50 case studies to recreate the total abundances of SOA and the contributions from the individual compound classes identified above [*Utembe et al.*, 2009]. Because the 14 representative species were based on MCM analogues making particularly important contributions to the total in each class, the effective atomic composition and functional group content were also well preserved. The SOA module has been updated in the present work by incorporating a degradation scheme for β-caryophyllene (representative of sesquiterpenes) into the CRI v2-R5 mechanism. The chemistry is a simplification of the first two generations of oxidation (as represented in the MCM v3.2 [*Jenkin et al.*, 2012]) as shown in Scheme 1 and in Table S1 in the supporting information. The addition of the degradation of β-caryophyllene includes 15 new chemical species, which take part in an additional 35 reactions. Among the 15 new species, six can partition to the condensed phase, and two are sufficiently nonvolatile to be assumed to be 100% in the condensed phase, these being C_{15} species containing four polar functional groups (see Scheme 1 and Table S2). After the first two generations, the chemistry feeds into the CRI α-pinene scheme, which is used as a mechanistic surrogate for the higher-generation chemistry. This forms a further three partitioning species (RTN25OOH, RTN24OOH, and RTN23OOH), which are representative C_9 species containing two, three, and four polar functional groups. The values of the partitioning coefficients applied to the newly implemented species are based on those of the closest MCM v3.2 analogues (Table S2). These were calculated from vapor pressures (Table S3) estimated by using the method of *Nannoolal et al.* [2008], in conjunction with species boiling temperatures estimated by the method of *Nannoolal et al.* [2004], as described by *Jenkin et al.* [2012].

The treatment of dry and wet deposition processes of the gas-phase species was described in detail by *Utembe et al.* [2011]. SOA and POA present in Lagrangian cells located within the boundary layer can also be lost through dry and wet depositions. The parameters of the dry deposition (e.g., deposition velocity over land and ocean) and wet deposition (dynamic and convective scavenging) of SOA and POA were

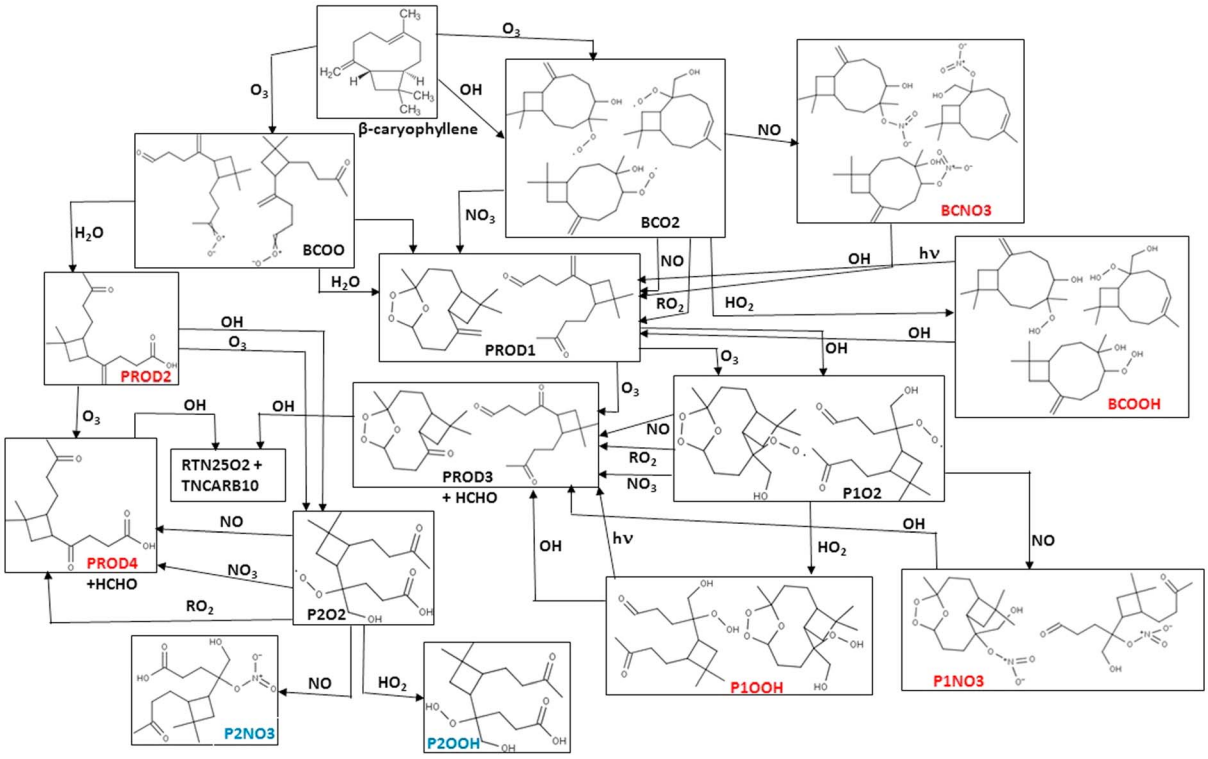

Scheme 1. The degradation mechanism of β-caryophyllene adopted in STOCHEM-CRI mechanisms. The compound partition to the condensed phase are shown in red, and the compounds assumed to transfer entirely to the condensed phase (P2NO3 and P2OOH) are shown in blue (gas-phase removal is not included for these species).

set equal to that of the nitrate aerosol, consistent with all components being present in a mixed aerosol under atmospheric condition. The deposition processes for the partitioning gas species were not included in these model runs.

The emissions data employed in the base case STOCHEM model were adapted from the Precursor of Ozone and their Effects in the Troposphere inventory [*Granier et al.*, 2005] for the year 1998. More details about the emissions data can be found in *Utembe et al.* [2011] and *Khan et al.* [2014]. The Base simulation, STOCHEM-Base performed, was based on the reference conditions used in the study of *Utembe et al.* [2011], which described biogenic SOA formation from 501 Tg/yr isoprene and 127 Tg/yr monoterpenes (α- and β-pinene). The simulation, STOCHEM-SQT1 was conducted, which involved the STOCHEM-Base being integrated after including global sesquiterpene emissions of 29 Tg/yr [*Guenther et al.*, 2012] with the chemistry of β-caryophyllene described above. *Guenther et al.* [2012] reported a range of global monoterpene emissions (157–177 Tg/yr) by using the Model of Emissions of Gases and Aerosols from Nature version 2.1 (MEGAN2.1) coupled with Community Land Model (CLM4) due to the different leaf area indexes (e.g., "satellite phenology" and "carbon nitrogen" configurations) used in the model. A simulation was performed which involved STOCHEM-SQT1 being integrated after including revised global monoterpene emissions of 162 Tg found for the year 2000 using MEGAN2.1 algorithms in CLM4 [*Guenther et al.*, 2012], this being an increase from the 127 Tg/yr applied by *Utembe et al.* [2011]; this run is subsequently referred as "STOCHEM-SQT'." One further integration (referred to as "STOCHEM-SQT2-PI") was performed for a preindustrial scenario, which involved the STOCHEM-SQT2 being integrated after removing anthropogenic emissions and reducing the biomass burning emissions from the model. Biomass burning emissions of CH_4, CO, SO_2, NO_x, and nonmethane VOCs (Table S4) have been scaled by using global scaling factors from the Edgar-Hyde emissions database [*van Aardenne et al.*, 2001]. More details about the preindustrial scenario can be found in *Khan et al.* [2015]. All simulations were run with meteorology from 1998 for a period of 24 months with the initial 12 months being discarded as a spin-up year.

Table 1. Global Burden and Production Terms for Simulated SOA in This Study and Their Comparison With Previous Studies

	Global Burden (Tg)	Production (Tg/Yr)
Base [*Utembe et al.*, 2011]	0.23	22.5
STOCHEM-SQT1	0.34	35.4
STOCHEM-SQT2	0.45	46.4
Henze and Seinfeld [2006]	0.39	16.4
Tsigaridis and Kanakidou [2007]	0.82	18.6
Hoyle et al. [2007]	0.52	55
Fu et al. [2008]	0.62[a]	29[a]
Henze et al. [2008]	0.81	30.3
Farina et al. [2010]	0.54	29.2
O'Donnell et al. [2011]	0.84	26.6
Spracklen et al. [2011]	1.84	140
Hodzic et al. [2016]	0.88 (2.31[b])	36.2 (132.0[b])
Lin et al. [2016]	1.06	55.4

[a]Reported in Tg carbon and converted here by using a 2:1 ratio of OM:OC.
[b]Semivolatile and intermediate volatility SOAs are included.

3. Results and Discussion

3.1. Global Budget of Biogenic SOA

The global burdens and production rates of simulated SOA from biogenic organic compounds for STOCHEM-SQT1 and STOCHEM-SQT2 cases are shown in Table 1. The global burden of SOA is found to be 0.34 Tg (an increment of 48% relative to the base case described in *Utembe et al.* [2011]) in STOCHEM-SQT1 due to the inclusion of the oxidation mechanisms of β-caryophyllene into the CRI mechanism. A further increase of SOA burden to 0.45 Tg (95% increase relative to the base case) in the simulation, STOCHEM-SQT2 is found when we increased the global monoterpene emissions from 127 Tg/yr to 162 Tg/yr. The simulated global burden of SOA in STOCHEM-SQT2 is found to be lower than those found in most recent modeling studies (Table 1). The SOA productions (46.4 Tg/yr, 106% increase relative to the base case) in STOCHEM-SQT2 fall within the ranges suggested by *Henze and Seinfeld* [2006], *Tsigaridis and Kanakidou* [2007], *Henze et al.* [2008], *Farina et al.* [2010], and *O'Donnell et al.* [2011] but lower than the values reported by *Hoyle et al.* [2007], *Spracklen et al.* [2011], *Lin et al.* [2016], and *Hodzic et al.* [2016] (Table 1).

The simulations performed by *Tsigaridis and Kanakidou* [2007] and *Hoyle et al.* [2007] considered the importance of other reactive volatile organic compounds (e.g., sesquiterpenes, terpenoid alcohols, and terpenoid ketones), ORVOC-derived SOA. The global emissions of ORVOC used in their model are approximately threefold to nine-fold higher than the emissions of sesquiterpenes used in our model, resulting in lower global burdens and SOA formation in our study. The SOA burden and SOA formation of *Spracklen et al.* [2011] is larger than our study because of the very large SOA source (100 Tg/yr) from a VOC precursor with emission pattern similar to anthropogenic CO emissions in their study. In our model, the oxidation of POA to SOA formation is not included, but *Spracklen et al.* [2011] estimated a substantial source of SOA (23 Tg/yr) from the oxidation of POA. The simulated SOA in this study is expected to be a lower limit as this representation only includes partitioning into organic aerosol. In reality, SOA can be formed by partitioning low-volatile organic gases onto low-volatility secondary organic products condensing onto particles across the size distribution [e.g., *Spracklen et al.*, 2008; D'Andrea et al., 2013; *Scott et al.*, 2014] or coarse particles like nitrates, dust, sea salt, and water droplets [*Mann et al.*, 2010] and from the irreversible uptake of gas-phase glyoxal, methylglyoxal, and isoprene epoxydiol [*Lin et al.*, 2016], which are not taken into account in our model. *Hoyle et al.* [2007] and *Tsigaridis and Kanakidou* [2003] considered the case that SOA could partition onto sulphate aerosol reporting increases of 25% and 85% in the global SOA production. *Fu et al.* [2008] showed that the glyoxal- and methylglyoxal-derived SOA increases the global SOA production by 60%; thus, the absence of their reactive uptake on aqueous aerosols in our model would worsen the model representation of SOA. Primary anthropogenic emissions of semivolatile/intermediate volatile organic compounds (S/IVOCs) can produce substantial quantities of SOA [*Pye and Seinfeld*, 2010; *Jathar et al.*, 2011; *Hodzic et al.*, 2016]. However, the global emissions of anthropogenic VOCs used in the model has no S/IVOCs emission data, which could support the lower limit of our SOA results. However, the work here is one of the first studies to consider a detailed oxidation mechanism of a sesquiterpene and the partitioning of its oxidized gas-phase product species onto organic aerosols.

In our model representation, we include only the O_3- and OH-initiated oxidation of β-caryophyllene without considering the oxidation by NO_3. Oxidation initiated by reaction with O_3 is simulated to be the dominant removal process (accounting for about 95% of its removal), and therefore the more important route to SOA formation. Further analysis suggests that products formed from both RO_2 + HO_2 reactions (e.g., P1OOH, P2OOH, and RTN23OOH) and RO_2 + NO reactions (e.g., P1NO3 and P2NO3) contribute to the simulated SOA, but with the former being significantly more important on a global scale. Consistent with this,

Table 2. Identities and Contributions (in Gg) of the SOA Biogenic Contributors to the Total Global Burden of SOA Simulated by STOCHEM-Base, STOCHEM-SQT1, and STOCHEM-SQT2[a]

Species	Description	Atomic Ratio, O/C	Mass Ratio, OM/OC	Base	SQT1	SQT2
RU12OOH	Second-generation isoprene product containing 2 –OH, –C(O) and –OOH groups	1.00	2.50	7.8	9.1 (15.8)	10.4 (32.6)
RTN28NO3	First-generation α-pinene product containing –OH and $–ONO_2$ groups	0.40	1.79	3.0	3.4 (12.8)	5.0 (65.8)
RTX28NO3	First-generation β-pinene product containing –OH and $–ONO_2$ groups	0.40	1.79	6.9	8.1 (18.0)	11.8 (71.5)
RCOOH25	First-/second-generation α-pinene product containing –C(O), –C(O)OH groups	0.30	1.53	12.6	14.7 (16.4)	21.9 (73.1)
RTN24OOH	Second-/third-generation α-pinene and β-caryophyllene product containing –OH, –C(O), and –OOH groups	0.44	1.74	51.1	68.3 (33.9)	95.0 (86.0)
RTX28OOH	First-generation β-pinene product containing –OH and –OOH groups	0.30	1.55	7.1	8.7 (22.2)	13.0 (82.8)
RTN28OOH	First-generation α-pinene product containing –OH and –OOH groups	0.30	1.55	2.3	3.0 (28.2)	4.5 (95.8)
RTN26OOH	Second-generation α-pinene product containing 2 –C(O) and –OOH groups	0.40	1.67	19.1	22.2 (16.2)	32.3 (69.1)
RTN26PAN	Second-generation α-pinene product containing –CO and $–C(O)OONO_2$ groups	0.60	2.04	2.8	3.4 (21.2)	4.9 (79.1)
RTN25OOH	Second-/third-generation α-pinene and β-caryophyllene product containing –C(O) and –OOH groups	0.33	1.59	1.6	2.8 (75.6)	4.0 (150.4)
RTN23OOH	Second-/third-generation α-pinene and β-caryophyllene product containing –OH, 2 –C(O), and –OOH groups	0.56	1.89	98.7	138.0 (39.9)	183.2 (85.6)
PROD2	First-generation β-caryophyllene oxidation product containing –C(O),––C = C–, and –C(O)OH groups	0.20	1.40	n/a	0.06	0.08
BCNO3	First-generation β-caryophyllene oxidation product containing –OH, –C = C–, and $–ONO_2$ groups	0.27	1.57	n/a	0.01	0.01
BCOOH	First-generation β-caryophyllene oxidation product containing –OH, –C = C–, and –OOH groups	0.20	1.41	n/a	0.12	0.14
P1NO3	Second-generation β-caryophyllene oxidation product containing −C(O), −OH, and −ONO2 groups	0.43	1.79	n/a	2.0	2.3
P1OOH	Second-generation β-caryophyllene oxidation product containing –C(O), –OH, and –OOH groups	0.37	1.63	n/a	12.5	14.2
PROD4	Second-generation β-caryophyllene oxidation product containing 2 –C(O) and –C(O)OH groups	0.29	1.51	n/a	3.5	4.0
P2NO3	Second-generation β-caryophyllene oxidation product containing –OH, –C(O), $–ONO_2$, and –C(O)OH groups	0.47	1.84	n/a	6.9	7.0
P2OOH	Second-generation β-caryophyllene oxidation product containing –OH, –C(O), –OOH, and –C(O)OH groups	0.40	1.68	n/a	15.9	16.0

[a]The percentage changes with respect to STOCHEM-Base are shown in parenthesis. n/a represents no available data. Percentage change = (STOCHEM-SQT–STOCHEM-base) * 100/STOCHEM-base.

analysis of the functional group content of biogenic SOA reveals important contributions from multifunctional hydroperoxides (also containing hydroxyl and carbonyl groups), the average per molecule for the SQT2 scenario being: $(–C(O)-)_{1.389}$, $(–OH)_{0.872}$, $(–OOH)_{0.838}$, $(–C(O)OH)_{0.099}$, $(–ONO_2)_{0.050}$, $(–C(O)OOH)_{0.038}$, $(–SOZ)_{0.013}$, and $(–C(O)OONO_2)_{0.009}$. The average empirical formula of the SOA in the SQT2 scenario is $C_{1.000}H_{1.744}O_{0.472}N_{0.006}$ (OM/OC = 1.78), this being slightly less oxygenated than that in the base case ($C_{1.000}H_{1.748}O_{0.485}N_{0.006}$, OM/OC = 1.80) because of the contribution of the larger organic species from β-caryophyllene degradation. These ratios lie well within the reported ranges for atmospheric and chamber SOA [*Aiken et al.*, 2008], with the individual contributors covering the ranges 0.2–1.0 for O/C and 1.4–2.5 for OM/OC (see Table 2). However, the ratios for the most abundant simulated SOA contributors lie in the narrower ranges 0.33–0.56 for O/C and 1.6–1.9 for OM/OC, suggesting that reported large contributions from ambient highly oxygenated material [e.g., *Aiken et al.*, 2008; *Chen et al.*, 2015] are not fully represented by our approach.

Table 2 shows the breakdown of simulated global SOA from biogenic organic compounds (e.g., isoprene, monoterpenes, and sesquiterpenes) into the representative species. The simulation results show that the higher-generation multifunctional species (RTN25OOH, RTN24OOH, and RTN23OOH), formed from both α-pinene and β-caryophyllene, contribute 66% to the total mass loading of SOA. These results therefore suggest that products of β-caryophyllene oxidation, formed over several generations, make significant contributions to the SOA burden. Whereas those formed from the first two generations of oxidation (by rapid sequential oxidation of the two double bonds) form SOA close to the emissions region, the higher-generation products identified above make significant contributions to SOA formation on much larger temporal and spatial scales. Compared with *Utembe et al.* [2011], STOCHEM-SQT1 shows the

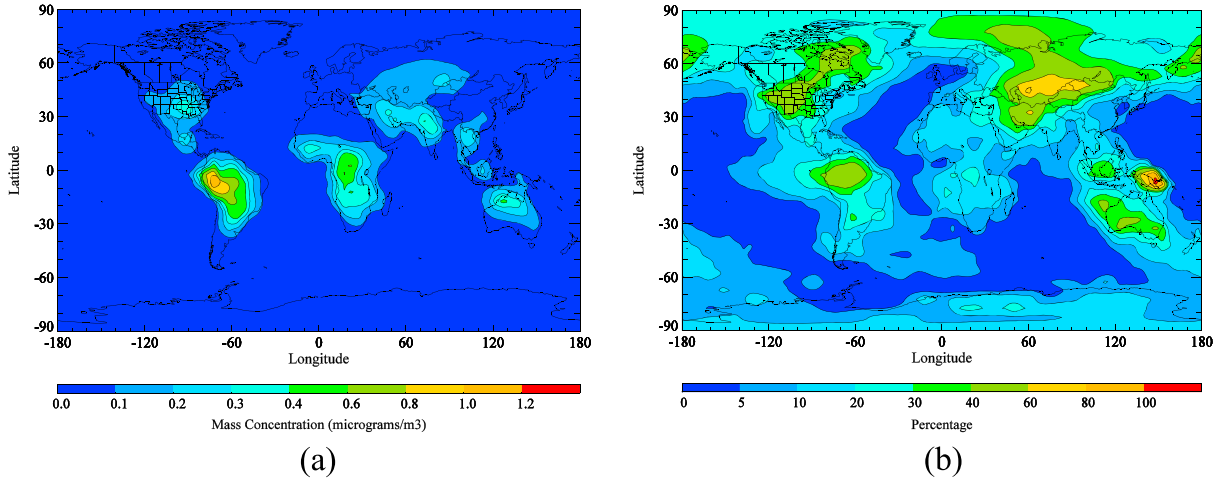

Figure 1. (a) The annual mean surface distribution of SOA increment after adding sesquiterpenes to the STOCHEM-base and (b) the percentage change of OA distribution simulated by the STOCHEM-SQT2 relative to the base case [*Utembe et al.*, 2011]. Percentage change = (STOCHEM-SQT2–STOCHEM-base) * 100/STOCHEM-Base.

increment of the global burdens of RTN25OOH-, RTN24OOH-, and RTN23OOH-derived SOAs by 76, 34, and 40%, respectively. This increase is primarily due to the additional formation of these representative species from β-caryophyllene oxidation, with a secondary effect being increased partitioning of all the species in Table 2 to the condensed phase due to the generally higher mass loadings of OA. The increased emissions of monoterpenes in the STOCHEM-SQT2 scenario further increase the condensed phase partitioning of all the species in Table 2, with particularly large increments (about 60%) for the oxidation products formed specifically from α-pinene and β-pinene. This illustrates the cumulative effect of adding sesquiterpenes and extra monoterpenes in the STOCHEM model.

3.2. Surface and Zonal Distribution of Sesquiterpene-Derived SOA

Figure 1a shows the surface distribution of SOA increment after adding sesquiterpenes (29 Tg/yr) in the STOCHEM-Base, and Figure 1b shows the percentage change of OA after adding sesquiterpenes and additional 35 Tg/yr monoterpenes in the STOCHEM-SQT1. In the model, SOA is formed by the partitioning of gas-phase species onto preexisting organic aerosol; therefore, the distribution of SOA is proportional to the amount of SOA precursors (see the surface distribution of monoterpenes and sesquiterpenes in Figure S1 in the supporting information). Globally, the species contributing to SOA are dominated by those formed from monoterpene and sesquiterpene oxidation (Table 2). Previous modeling studies of SOA using STOCHEM-CRI [*Utembe et al.*, 2009, 2011] showed the formation of SOA from a series of first-, second-, and third-generation oxidation products of monoterpenes (90%), isoprene (3%), and aromatic species (7%) and found the highest concentrations of SOA by up to 3.0 $\mu g/m^3$ over South America and central Africa. However, including 29 Tg/yr sesquiterpenes (approximately a factor of 5 lower than the global emission of monoterpenes) increases the simulated SOA concentrations by up to 1.2 $\mu g/m^3$, which is about 30% to the total SOA formation in the model. The surface distribution of sesquiterpene-derived SOA follows a similar trend to those of SOA formation from the other biogenic VOCs [*Utembe et al.*, 2011]. Central Africa and South America have a significant biomass burning season, but this is co-located with high levels of sesquiterpene emissions resulting in changes of SOA concentrations reaching up to 1.2 $\mu g/m^3$ (Figure 1a). Sesquiterpenes and the additional monoterpenes in the STOCHEM-SQT2 scenario (35 Tg/yr) increased the concentrations of OA by 60 to 80% over parts of South America, northern Asia, Russia, Indonesia, and North America (Figure 1b). In South America, the high emissions of sesquiterpenes and monoterpenes (Figure S1) and the large local source of POA from biomass burning led to significant increments in OA concentrations. The tropical regions of the Philippines, India, and Indonesia produce high levels of biogenic emissions. The large local sources of POA from Australia and South Asia resulted in increased of OA concentrations. The high levels of SOA precursors (including biogenic and anthropogenic) in northern Asia, Russia, central U.S., and Canada lead to increased SOA formation despite the relatively low POA concentrations, and hence, SOA was a significant fraction of the total OA in these regions.

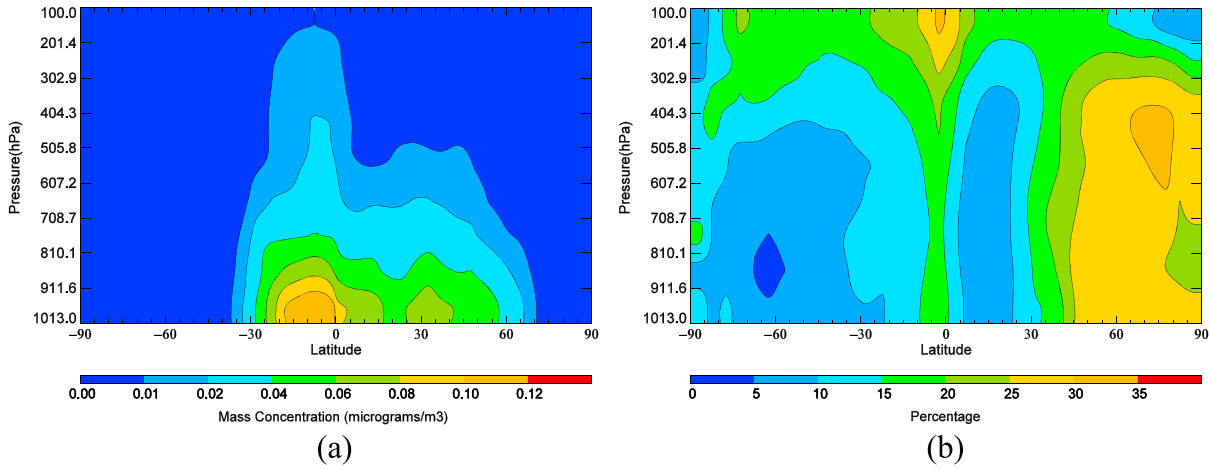

Figure 2. (a) The annual and zonal mean distributions of SOA increment after adding sesquiterpenes to the STOCHEM-base and (b) the percentage change of zonal OA simulated by STOCHEM-SQT2 relative to the base case [*Utembe et al.*, 2011]. Percentage change = (STOCHEM-SQT2–STOCHEM-base) * 100/STOCHEM-Base.

The zonal distribution of SOA from sesquiterpenes showed a peak (0.12 $\mu g/m^3$) at the surface between 0° and 20°S because of the high emissions of sesquiterpenes in the tropical regions combined with large sources of POA from biomass burning. The distribution showed a greater overall SOA concentrations in the northern hemisphere compared with the southern hemisphere (Figure 2a) because of the greater landmass in the northern hemisphere. Generally, SOA concentrations decrease with increasing altitude because of their removal by wet and dry depositions. However, consistent levels of sesquiterpene-derived SOA (0.04 $\mu g/m^3$) was found up to 400 hPa in the tropics (Figure 2a). The quantities at higher altitudes resulted from the transport of gas-phase multigeneration oxidation products to the upper troposphere, where they preferentially partitioned onto preexisting organic aerosol because of the lower temperatures. The STOCHEM-SQT2 integration saw an increase in the concentrations of OA up to 30% in the tropical upper troposphere. This was caused by the large biogenic emissions of sesquiterpenes and monoterpenes, which are mostly in the equatorial region and the multigeneration chemistry resulting in significant SOA in the upper troposphere. The most significant increase of OA by up to 30% was found between 50°N and 90°N up to 300 hPa (Figure 2b). The gas-phase oxidation products due to the increased global emissions of sesquiterpenes and monoterpenes saturated the partitioning medium, POA in the lower troposphere, and the remaining SOA precursors transported above the surface layer, ultimately condensed to the aerosol phase at higher altitude.

3.3. Model Evaluation

We compare model simulations with a suite of OA flight campaign measurements compiled from *Heald et al.* [2011] to evaluate our model results. Figure 3 compares the mean vertical profiles of OA measured during 16 individual flight campaigns and modeled by STOCHEM-Base, STOCHEM-SQT1, and STOCHEM-SQT2. Five of these campaigns are representative of remote conditions (VOCALS-UK, OP3, ITOP, IMPEX, and TROMPEX), and four of these campaigns (DABEX/DODO, AMMA, ARCTAS-summer, and ARCTAS-spring) were influenced by biomass burning activities; however, the campaigns ACE-Asia, TexAQS, ADIENT, EUCAARI, and ADRIEX were performed to study regional anthropogenic pollution events and the remaining two campaigns (MILAGRO and ITCT-2 K4) were conducted at the regions which were heavily influenced by both regional pollution and biomass burning plumes. Similar to the comparisons presented by *Utembe et al.* [2011], the OA concentrations simulated in the STOCHEM-Base scenario provide a generally good description of the observed vertical profiles but with the absolute concentrations being systematically underestimated. The mean biases (MB) and normalized mean biases (NMB) between modeled and observed data were found to be -0.26 $\mu g/m^3$ and 52% for remote regions, -1.69 $\mu g/m^3$ and 68% for biomass burning dominating regions, -2.03 $\mu g/m^3$ and 76% for anthropogenically polluted regions, and -2.80 $\mu g/m^3$ and 82% for both biomass burning plumes and anthropogenically polluted regions. The diminishing level of agreement for polluted regions (Figure 3) is at least partly due to the coarse model resolution (5° × 5°), which cannot fully resolve typical biomass burning plumes or regional pollution. However, for remote regions, the MBs are much smaller (eightfold to tenfold lower than

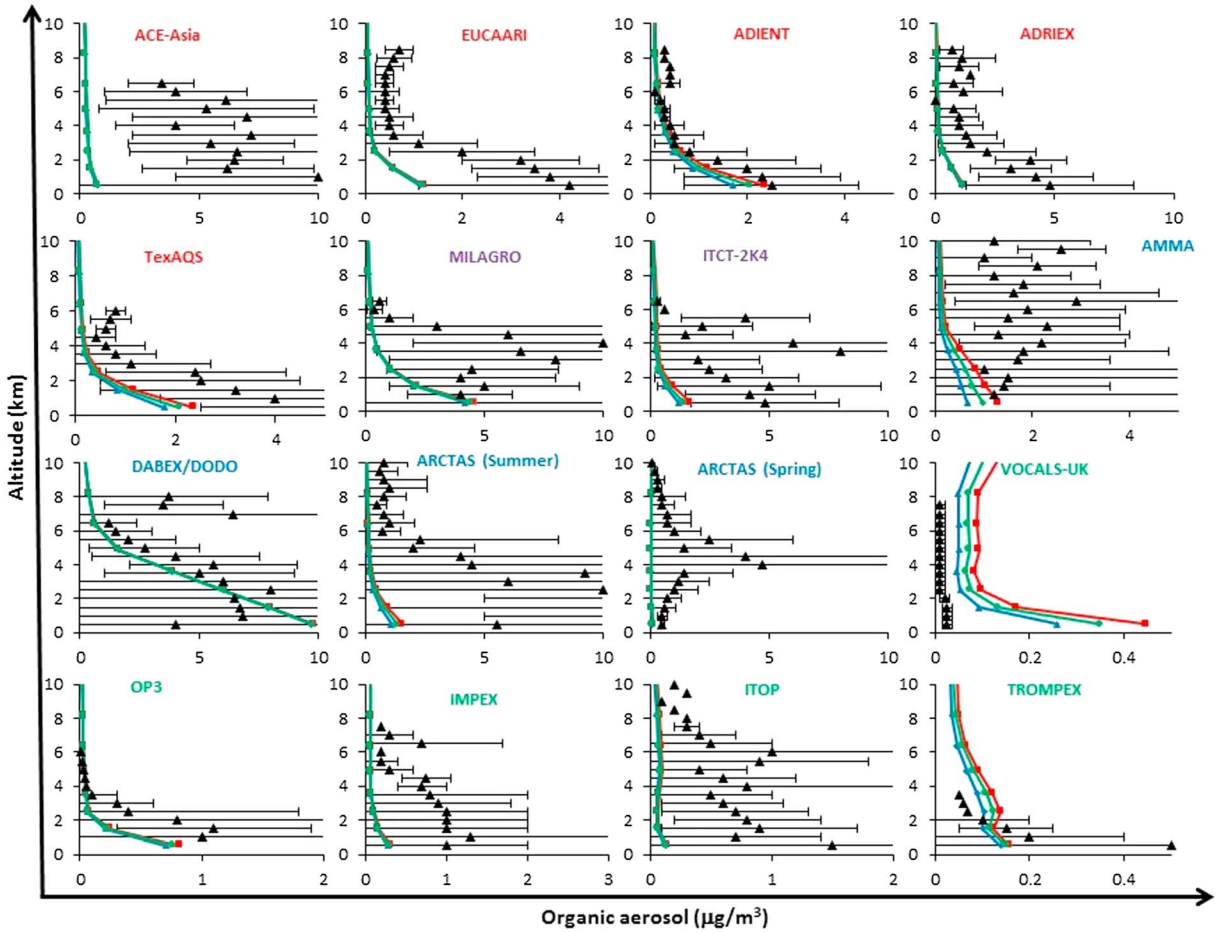

Figure 3. Vertical profiles for measured and modeled organic aerosols. The flight campaigns with green, blue, red, and violet fonts represent remote, biomass burning plumes, anthropogenically polluted, and biomass burning plumes + anthropogenically polluted regions, respectively. The blue, green, and red lines represent mean model values of OA produced by STOCHEM-Base, STOCHEM-SQT1, and STOCHEM-SQT2, respectively. The black triangles represent the measurement OA data, and the black bars represent the measurement variability.

the polluted regions), suggesting a greater suitability of the STOCHEM-SQT model for the modeling of OA in free troposphere. The simulated OA concentrations show a slightly improved agreement with the observations (6–12% for remote locations and 2–4% for anthropogenic and biomass burning locations) after adding sesquiterpenes (STOCHEM-SQT1) and extended monoterpenes (STOCHEM-SQT2) in the model. More flight campaigns covering the vegetation regions (e.g., Amazon rainforest, southern Africa, and north Australia) would be invaluable to help improving model representation.

As indicated above in section 3.1, and in *Utembe et al.* [2011], there are a number of potential contributors to the general underestimation of OA levels, deriving from uncertainties and possible omissions in the representations of both POA emissions and processes involved in SOA formation. However, the results further illustrate that sesquiterpene oxidation products supplement SOA formation in rural and remote regions, with a simulated contribution that is comparable to SOA formed from monoterpene oxidation. This is consistent with the results of studies that have inferred SOA contributions from detection of tracers formed from β-caryophyllene and α-pinene oxidation at a number of locations [*Jaoui et al.*, 2007; *Kleindienst et al.*, 2007; *Parshintsev et al.*, 2008].

Figure 4 shows the model evaluation with 25 surface measurement data from sites having different atmospheric conditions (e.g., urban, urban downwind, and remote/rural) compiled from *Zhang et al.* [2007]. The seasonal cycle of OA can be dominated by the presence of biogenic SOA, whose production maximizes during summer because of enhanced photochemistry and higher precursors (e.g., isoprene, monoterpenes, and sesquiterpenes) emissions. However, the production of POA is dominated during the biomass burning season, e.g., December to March for north Africa and South Asia and June to October for South America

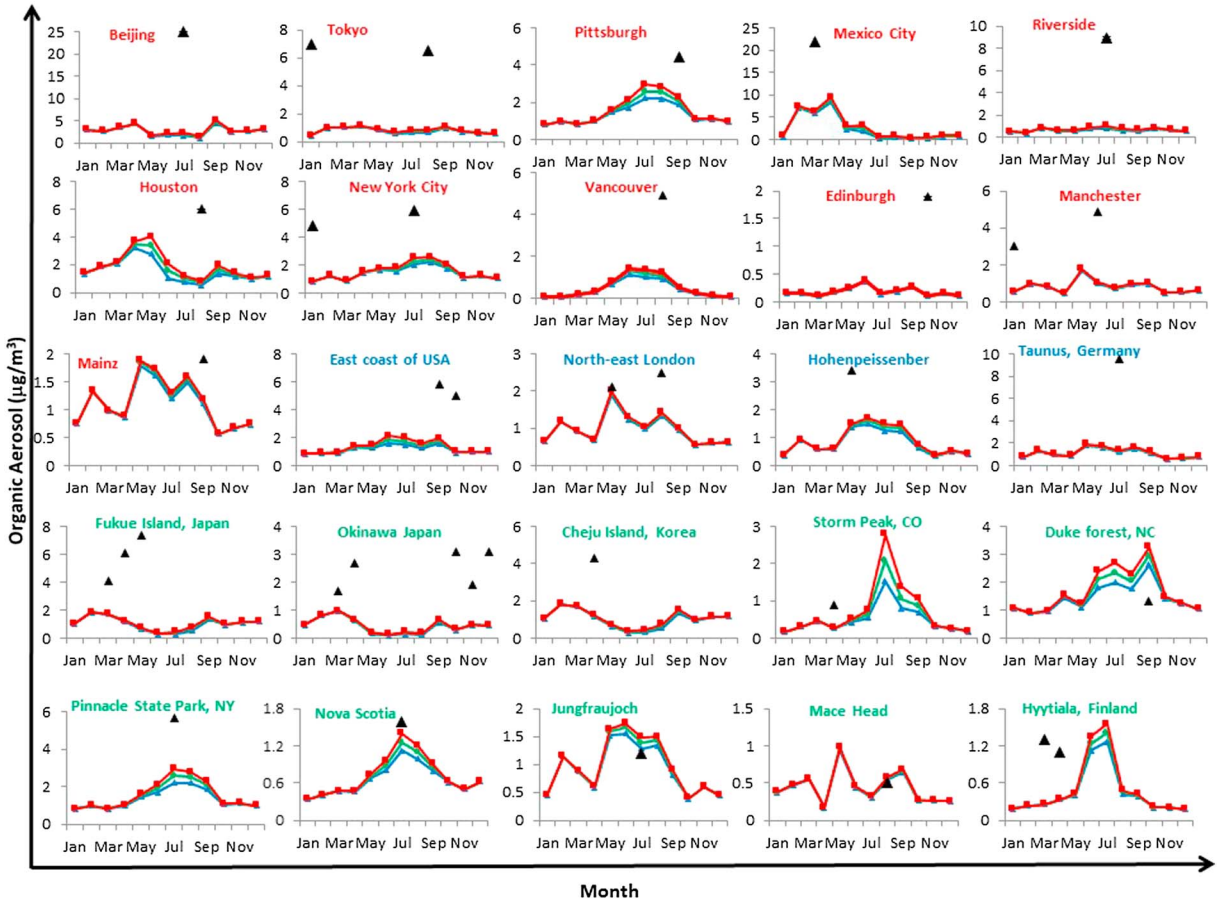

Figure 4. Monthly variations of the surface OA concentrations of selected monitoring stations. The stations with red, blue, and green fonts represent urban, urban downwind, and rural/remote sites, respectively.The blue, green, and red lines of individual plots represent mean modeled OA produced by STOCHEM-Base, STOCHEM-SQT1, and STOCHEM-SQT2, respectively. The black triangle symbols represent the observed OA.

and south Africa [*Cooke*, 2010]. The combination of these two processes leads to a complex seasonal cycle for model OA. The model base case simulation underpredicted OA concentrations by on average 6.5 $\mu g/m^3$ (NMB 82%) for urban, 3.3 $\mu g/m^3$ (NMB 70%) for urban downwind, and 1.9 $\mu g/m^3$ (NMB 45%) for remote/rural sites. The underprediction for urban downwind and rural/remote sites was comparable with previous boundary layer simulated to observed ratios from other studies [*Heald et al.*, 2005; *McKeen et al.*, 2007; *Matsui et al.*, 2009]. The global model is not the best tool to study urban aerosol levels [*Tsigaridis et al.*, 2014], so a large underestimation of the model compared with measurements is found for urban areas. The most significant differences are for Beijing, Tokyo, and Mexico City. There has been significant increase in industrialization of Asia since 1998 leading to large increases in anthropogenic emissions [*Liu et al.*, 2003]. The large changes in Asian emissions of POA since 1998 are not captured by the model. Considering S/IVOC-derived SOA into the STOCHEM-SQT model could potentially improve the discrepancies between model, and measurement for urban sites as *Hodzic et al.* [2010] found modeled SOA much closer to observations at Mexico City when intermediate-volatility organics were taken into account in their CHIMERE model. The coarse emission grids, underestimation in emissions of precursor gases to SOA and over simplification of gas to aerosol partitioning, can be the other reasons for measurement-model discrepancies.

For remote environments, where the air is clean and the emission levels of SOA precursors are low, the model-measurement agreement is found to be good for the rural/remote sites (e.g., Nova Scotia, Jungfraujoch, Mace Head, Storm Peak, and Duke Forest). Including sesquiterpenes in the model reduces the underprediction by 2% for urban/urban downwind areas and 4% for remote/rural areas, and increased monoterpene global emissions reduce the underprediction further by 2% for urban/urban downwind areas and 3% for remote/rural areas.

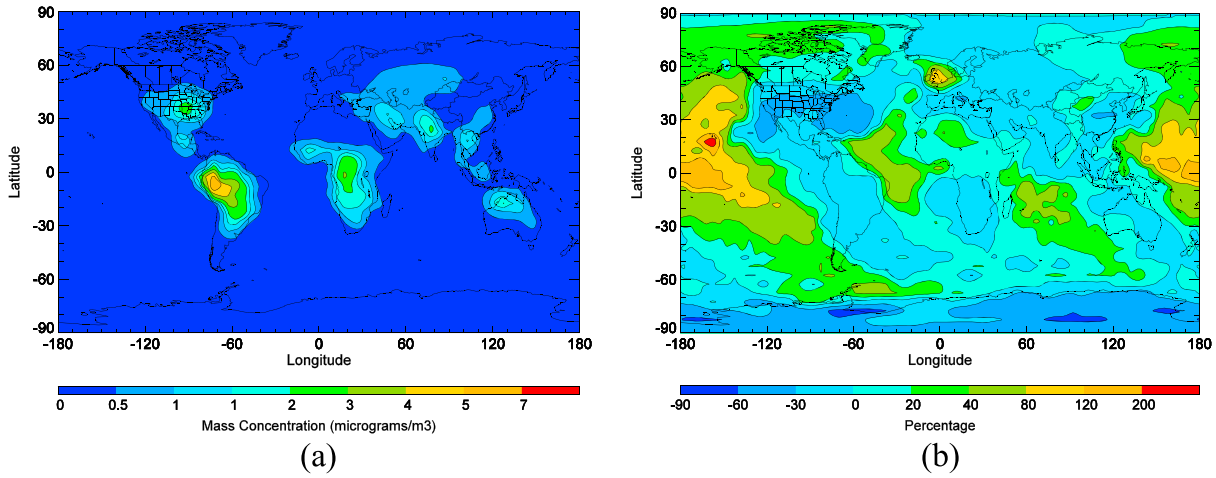

Figure 5. (a) The annual mean surface distribution of SOA simulated by the STOCHEM-SQT2-PI and (b) the percentage change of SOA distribution from preindustrial to present case. Percentage change = (STOCHEM-SQT2–STOCHEM-SQT2-PI) * 100/STOCHEM-SQT2-PI.

3.4. Preindustrial Versus Present

The global distribution of SOA concentration in preindustrial scenario after adding sesquiterpenes and extended monoterpenes are shown in Figure 5. The maximum concentrations of SOA up to 7 $\mu g/m^3$ for preindustrial scenario were found over South America (Figure 5a). The percentage change of SOA from preindustrial to present scenario showed that SOA levels had increased up to 200% over the tropical ocean. HO_x and O_3 levels over tropical oceans were significantly increased since the preindustrial period (see Figure S2). This had the effect of increasing oxidation of SOA precursors (e.g., monoterpenes and sesquiterpenes) by OH and O_3, resulting in increased SOA over tropical oceans (Figure 5b).

4. Conclusion

The degradation mechanisms of sesquiterpenes have been added to the aerosol module of CRI v2-R5 chemical mechanism and employed in a global chemistry transport model, STOCHEM to investigate the formation of SOA from sesquiterpenes using β-caryophyllene as a representative species. After adding sesquiterpenes and revising the global emissions of monoterpenes in the model, we estimated the revised global production of SOA as 46.4 Tg/yr, which fell within the range of most previous modeling studies. The addition of sesquiterpene emissions increased the simulated SOA concentrations by up to 1.2 $\mu g/m^3$. The highest concentrations of sesquiterpene-derived SOA were found over central Africa and South America. Consistent with earlier findings [*Utembe et al.*, 2011], the comparison of simulated and measured organic aerosol revealed that STOCHEM-SQT still generally underpredicts OA but supports an important role for multigenerational oxidation in sustaining SOA formation in the free troposphere.

The sesquiterpene degradation chemistry used within this representation is novel with regard to other previous global model studies; in that it provides an explicit representation of the complete gas-phase degradation of β-caryophyllene. The results suggest that products formed over several generations of oxidation make significant contributions to SOA formation. Those formed from the first two generations of oxidation (by rapid sequential oxidation of the two double bonds) have been reported to be important in chamber studies [e.g., *Li et al.*, 2011], but the present work suggests that higher generation products make particularly significant contributions to atmospheric SOA formation on much longer time scales. Experimental or theoretical elucidation of the further gas-phase oxidation of more volatile second generation products would therefore be of value.

Analysis of the functional group content of the simulated biogenic SOA reveals important contributions from multifunctional hydroperoxides (also containing hydroxyl and carbonyl groups), which are generally formed from reactions of HO_2 with oxygenated peroxy radicals in the atmosphere. The simulated ratios, O/C and OM/OC, for the compounds making the most abundant contributions to SOA lie in the respective ranges 0.33–0.56 and 1.6–1.9. These lie within the reported ranges for atmospheric and chamber SOA

but suggest that reported large contributions from ambient highly oxygenated material [e.g., *Aiken et al.*, 2008; *Chen et al.*, 2015] are not fully represented by our approach. Further information on mechanisms forming highly oxygenated products, and validated representations for use in reduced atmospheric mechanisms, are therefore required.

In addition to the above, future developments of the organic aerosol representation in STOCHEM-SQT will consider a number of improvements including partitioning of organic gases onto coarse particles like nitrates, sulphates, dust, sea salt, and uptake into water droplets, updating the isoprene chemistry with considering the epoxide species as SOA contributors, aqueous phase photooxidation of glyoxal and methylglyoxal, and oxidation of low vapor pressure intermediate-volatility and semivolatile organic compounds. With regard to the wider context, more field and flight measurements, especially over South America, southern Africa, and north Australia would be invaluable to help improve model representations.

Acknowledgments
We thank NERC and Bristol ChemLabS under whose auspices various aspects of this work was funded. All flight and field measurement data sets used in this paper are properly cited and referred to in the reference list. Supporting data for model runs are included as four tables in the supporting information; any additional data can be obtained from the authors upon request (anwar.khan@bristol.ac.uk).

References

Aiken, A. C., et al. (2008), O/C and OM/OC ratios of primary, secondary, and ambient organic aerosols with high-resolution time-of-flight aerosol mass spectrometry, *Environ. Sci. Technol.*, *42*, 4478–4485, doi:10.1021/es703009q.

Alfarra, M. R., J. F. Hamilton, K. P. Wyche, N. Good, M. W. Ward, T. Carr, M. H. Barley, P. S. Monks, M. E. Jenkin, and G. B. McFiggans (2012), The effect of photochemical ageing and initial precursor concentration on the composition and hygroscopic properties of β-caryophyllene secondary organic aerosol, *Atmos. Chem. Phys.*, *12*, 6417–6436, doi:10.5194/acp-12-6417-2012.

Atkinson, R., and J. Arey (2003), Atmospheric degradation of volatile organic compounds, *Chem. Rev.*, *103*, 4605–4638, doi:10.1021/cr0206420.

Calogirou, A., D. Kotzias, and A. Kettrup (1997), Product analysis of the gas-phase reaction of beta-caryophyllene with ozone, *Atmos. Environ.*, *31*, 283–285, doi:10.1016/1352-2310(96)00190-2.

Carlton, A. G., C. Wiedinmyer, and J. H. Kroll (2009), A review of secondary organic aerosol (SOA) formation from isoprene, *Atmos. Chem. Phys.*, *9*, 4987–5005, doi:10.5194/acp-9-4987-2009.

Carlton, A. G., P. V. Bhave, S. L. Napelenok, E. D. Edney, G. Sarwar, R. W. Pinder, G. A. Pouliot, and M. Houyoux (2010), Model representation of secondary organic aerosol in CMAQv4.7, *Environ. Sci. Technol.*, *44*, 8553–8560, doi:10.1021/es100636q.

Carlton, A. G., B. J. Turpin, K. E. Altieri, S. Seitzinger, A. Reff, H. J. Lim, and B. Ervens (2007), Atmospheric oxalic acid and SOA production from glyoxal: Results of aqueous photooxidation experiments, *Atmos. Environ.*, *41*, 7588–7602, doi:10.1016/j.atmosenv.2007.05.035.

Chan, M. N., et al. (2011), Influence of aerosol acidity on the chemical composition of secondary organic aerosol from β-caryophyllene, *Atmos. Chem. Phys.*, *11*, 1735–1751, doi:10.5194/acp-11-1735-2011.

Chen, Q., et al. (2015), Elemental composition of organic aerosol: The gap between ambient and laboratory measurements, *Geophys. Res. Lett.*, *42*, 4182–4189, doi:10.1002/2015GL063693.

Cooke, M. C. (2010), Global modelling of atmospheric trace gases using the CRI mechanism, PhD Thesis, Univ. of Bristol, U. K.

D'Andrea, S. D., S. A. K. Häkkinen, D. M. Westervelt, C. Kuang, E. J. T. Levin, V. P. Kanawade, W. R. Leaitch, D. V. Spracklen, I. Riipinen, and J. R. Pierce (2013), Understanding global secondary organic aerosol amount and size-resolved condensational behaviour, *Atmos. Chem. Phys.*, *13*, 11519–11534, doi:10.5194/acp-13-11519-2013.

Ervens, B., A. G. Carlton, B. J. Turpin, K. E. Altieri, S. M. Kreidenweis, and G. Feingold (2008), Secondary organic aerosol yields from cloud-processing of isoprene oxidation products, *Geophys. Res. Lett.*, *35*, L02816, doi:10.1029/2007GL031828.

Ervens, B., B. J. Turpin, and R. J. Weber (2011), Secondary organic aerosol formation in cloud droplets and aqueous particles (aqSOA): A review of laboratory, field and model studies, *Atmos. Chem. Phys.*, *11*, 11069–11102, doi:10.5194/acp-11-11069-2011.

Farina, S. C., P. J. Adams and S. N. Pandis (2010), Modeling global secondary organic aerosol formation and processing with the volatility basis set: Implications for anthropogenic secondary organic aerosol, *J. Geophys. Res.*, *115*, D09202, doi:10.1029/2009JD013046.

Fu, T.-M., D. J. Jacob, F. Wittrock, J. P. Burrows, M. Vrekoussis and D. K. Henze (2008), Global budgets of atmospheric glyoxal and methylglyoxal, and implications for formation of secondary organic aerosols, *J. Geophys. Res.*, *113*, D15303, doi:10.1029/2007JD009505.

Goldstein, A. H., and I. E. Galbally (2007), Known and unexplored organic constituents in the Earth's atmosphere, *Environ. Sci. Technol.*, *41*, 1514–1521, doi:10.1021/es072476p.

Granier, C., J. F. Lamarque, A. Mieville, J. F. Muller, J. Olivier, J. Orlando, J. Peters, G. Petron, S. Tyndall and S. Wallens (2005), POET, a database of surface emissions of ozone precursors. [Available at http://accent.aero.jussieu.fr/database_table_inventories.php.]

Griffin, R. J., D. R. Cocker, R. C. Flagan, and J. H. Seinfeld (1999), Organic aerosol formation from oxidation of biogenic hydrocarbons, *J. Geophys. Res.*, *104*, 3555–3567, doi:10.1029/1998JD100049.

Guenther, A. B., X. Jiang, C. L. Heald, T. Sakulyanontvittaya, T. Duhl, L. K. Emmons, and X. Wang (2012), The model of emissions of gases and aerosols from nature version 2.1 (MEGAN2.1): An extended and updated framework for modeling biogenic emissions, *Geosci. Model Dev.*, *5*, 1471–1492, doi:10.5194/gmd-5-1471-2012.

Hallquist, M., et al. (2009), The formation, properties and impact of secondary organic aerosol: Current and emerging issues, *Atmos. Chem. Phys.*, *9*, 5155–5236, doi:10.5194/acp-9-5155-2009.

Heald, C. L., D. J. Jacob, R. J. Park, L. M. Russell, B. J. Huebert, J. H. Seinfeld, H. Liao and R. J. Weber (2005), A large organic aerosol source in the free troposphere missing from current models, *Geophys. Res. Lett.*, *32*, GL023831, doi:10.1029/2005GL023831.

Heald, C. L., et al. (2011), Exploring the vertical profile of atmospheric organic aerosol: Comparing 17 aircraft field campaigns with a global model, *Atmos. Chem. Phys.*, *11*, 12673–12696, doi:10.5194/acp-11-12673-2011.

Henze, D. K., and J. H. Seinfeld (2006), Global secondary organic aerosol from isoprene oxidation, *Geophys. Res. Lett.*, *33*, L09812, doi:10.1029/2006GL025976.

Henze, D. K., J. H. Seinfeld, N. L. Ng, J. H. Kroll, T. M. Fu, D. J. Jacob, and C. L. Heald (2008), Global modelling of secondary organic aerosol formation from aromatic hyrocarbons: High vs low-yields pathways, *Atmos. Chem. Phys.*, *8*, 2405–2420, doi:10.5194/acp-8-2405-2008.

Hildebrandt, L., N. M. Donahue, and S. N. Pandis (2009), High formation of secondary organic aerosol from the photo-oxidation of toluene, *Atmos. Chem. Phys.*, *9*, 2973–2986, doi:10.5194/acp-9-2973-2009.

Hodzic, A., P. S. Kasibhatla, D. S. Jo, C. D. Cappa, J. L. Jimenez, S. Madronich, and R. J. Park (2016), Rethinking the global secondary organic aerosol (SOA) budget: Stronger production, faster removal, shorter lifetime, *Atmos. Chem. Phys.*, *16*, 7917–7941, doi:10.5194/acp-16-7917-2016.

Hodzic, A., J. L. Jimenez, S. Madronich, M. R. Canagaratna, P. F. DeCarlo, L. Kleinman, and J. Fast (2010), Modeling organic aerosols in a megacity: Potential contribution of semi-volatile and intermediate volatility primary organic compounds to secondary organic aerosol formation, *Atmos. Chem. Phys.*, *10*, 5491–5514, doi:10.5194/acp-10-5491-2010.

Hoffmann, T., J. R. Odum, F. Bowman, D. Collins, D. Klockow, R. C. Flagan, and J. H. Seinfeld (1997), Formation of organic aerosols from the oxidation of biogenic hydrocarbons, *J. Atmos. Chem.*, *26*, 189–222, doi:10.1023/A:1005734301837.

Hoyle, C. R., T. Berntsen, G. Myhre, and I. S. A. Isaksen (2007), Secondary organic aerosol in the global aerosol-chemical transport model Oslo CTM2, *Atmos. Chem. Phys.*, *7*, 5675–5694, doi:10.5194/acp-7-5675-2007.

IPCC (2013), Climate change 2013: The physical science basis, in *Contribution of Working Group I to the Fifth Assessment Report of the Intergovernmental Panel on Climate Change (IPCC)*, edited by T. F. Stocker et al., pp. 571–657, Cambridge Univ. Press, Cambridge, U. K., and New York.

Jaoui, M., S. Leungsakul, and R. M. Kamens (2003), Gas and particle products distribution from the reaction of β-caryophyllene with ozone, *J. Atmos. Chem.*, *45*, 261–287, doi:10.1023/A:1024263430285.

Jaoui, M., K. G. Sexton, and R. M. Kamens (2004), Reaction of α-cedrene with ozone: Mechanism, gas and particulate products distribution, *Atmos. Environ.*, *38*, 2709–2725, doi:10.1016/j.atmosenv.2004.02.007.

Jaoui, M., M. Lewandowski, T. E. Kleindienst, J. H. Offenberg and E. O. Edney (2007), β-caryophyllinic acid: An atmospheric tracer for β-caryophyllene secondary organic aerosol, *Geophys. Res. Lett.*, *34*, L05816, doi:10.1029/2006GL028827.

Jardine, K., et al. (2011), Within-canopy sesquiterpene ozonolysis in Amazonia, *J. Geophys. Res.*, *116*, D19301, doi:10.1029/2011JD016243.

Jathar, S. H., S. C. Farina, A. L. Robinson, and P. J. Adams (2011), The influence of semi-volatile and reactive primary emissions on the abundance and properties of global organic aerosol, *Atmos. Chem. Phys.*, *11*, 7727–7746, doi:10.5194/acp-11-7727-2011.

Jenkin, M. E., L. A. Watson, S. R. Utembe, and D. E. Shallcross (2008), A Common Representative Intermediate (CRI) mechanism for VOC degradation. Part 1: Gas phase mechanism development, *Atmos. Environ.*, *42*, 7185–7195, doi:10.1016/j.atmosenv.2008.07.028.

Jenkin, M. E., K. P. Wyche, C. J. Evans, T. Carr, P. S. Monks, M. R. Alfarra, M. H. Barley, G. B. McFiggans, J. C. Young, and A. R. Rickard (2012), Development and chamber evaluation of the MCM v3.2 degradation scheme for β-caryophyllene, *Atmos. Chem. Phys.*, *12*, 5275–5308, doi:10.5194/acp-12-5275-2012.

Jimenez, J. L., et al. (2009), Evolution of organic aerosols in the atmosphere, *Science*, *326*, 1525–1529, doi:10.1126/science.1180353.

Johns, T. C., R. E. Carnell, J. F. Crossley, J. M. Gregory, J. F. B. Mitchell, C. A. Senior, S. F. B. Tett, and R. A. Wood (1997), The second Hadley Centre coupled ocean-atmosphere GCM: Model description, spinup and validation, *Climate Dyn.*, *13*, 103–134, doi:10.1007/s003820050155.

Kanawati, B., F. Herrmann, S. Joniec, R. Winterhalter, and G. K. Moortgat (2008), Mass spectrometric characterization of β-caryophyllene ozonolysis products in the aerosol studied using an electrospray triple quadrupole and time-of-flight analyzer hybrid system and density functional theory, *Rapid Commun. Mass Spectrom.*, *22*, 165–186, doi:10.1002/rcm.3340.

Khan, M. A. H., et al. (2014), Reassessing the photochemical production of methanol from peroxy radical self and cross reactions using the STOCHEM-CRI global chemistry and transport model, *Atmos. Environ.*, *99*, 77–84, doi:10.1016/j.atmosenv.2014.09.056.

Khan, M. A. H., M. C. Cooke, S. R. Utembe, A. T. Archibald, R. G. Derwent, P. Xiao, C. J. Percival, M. E. Jenkin, W. C. Morris, and D. E. Shallcross (2015), Global modeling of the nitrate radical (NO_3) for present and pre-industrial scenarios, *Atmos. Res.*, *164-165*, 347–357, doi:10.1016/j.atmosres.2015.06.006.

Kleindienst, T. E., M. Jaoui, M. Lewandowski, J. H. Offenberg, C. W. Lewis, P. V. Bhave, and E. O. Edney (2007), Estimates of the contributions of biogenic and anthropogenic hydrocarbons to secondary organic aerosol at a southeastern US location, *Atmos. Environ.*, *41*, 8288–8300, doi:10.1016/j.atmosenv.2007.06.045.

Kroll, J. H., and J. H. Seinfeld (2008), Chemistry of secondary organic aerosol: Formation and evolution of low-volatility organics in the atmosphere, *Atmos. Environ.*, *42*, 3593–3624, doi:10.1016/j.atmosenv.2008.01.003.

Kroll, J. H., N. L. Ng, S. M. Murphy, V. Varutbangkul, R. C. Flagan and J. H. Seinfeld (2005), Chamber studies of secondary organic aerosol growth by reactive uptake of simple carbonyl compounds, *J. Geophys. Res.*, *110*, D23207, doi:10.1029/2005JD006004.

Kroll, J. H., N. L. Ng, S. M. Murphy, R. C. Flagan, and J. H. Seinfeld (2006), Secondary organic aerosol formation from isoprene photooxidation, *Environ. Sci. Technol.*, *40*, 1869–1877, doi:10.1021/es0524301.

Lane, T. E., N. M. Donahue, and S. N. Pandis (2008), Simulating secondary organic aerosol formation using the volatility basis-set approach in a chemical transport model, *Atmos. Environ.*, *42*, 7439–7451, doi:10.1016/j.atmosenv.2008.06.026.

Lee, A., A. H. Goldstein, M. D. Keywood, S. Gao, V. Varutbangkul, R. Bahreini, N. L. Mg, R. C. Flagan and J. H. Seinfeld (2006a), Gas-phase products and secondary aerosol yields from the ozonolysis of ten different terpenes, *J. Geophys. Res.*, *111*, D07302, doi:10.1029/2005JD006437.

Lee, A., A. H. Goldstein, J. H. Kroll, N. L. Ng, V. Varutbangkul, R. C. Flagan and J. H. Seinfeld (2006b), Gas-phase products and secondary aerosol yields from the photooxidation of 16 different terpenes, *J. Geophys. Res.*, *111*, D17305, doi:10.1029/2006JD007050.

Li, J., M. Cleveland, L. D. Ziemba, R. J. Griffin, K. C. Barsanti, J. F. Pankow, and Q. Ying (2015), Modeling regional secondary organic aerosol using the Master Chemical Mechanism, *Atmos. Environ.*, *102*, 52–61, doi:10.1016/j.atmosenv.2014.11.054.

Li, L., P. Tang, S. Nakao, C.-L. Chen, and D. R. Cocker III (2016), Role of methyl group number on SOA formation from monocyclic aromatic hydrocarbons photooxidation under low-NO_x conditions, *Atmos. Chem. Phys.*, *16*, 2255–2272, doi:10.5194/acp-16-2255-2016.

Li, Y. J., Q. Chen, M. I. Guzman, C. K. Chan, and S. T. Martin (2011), Second-generation products contribute substantially to the particle-phase organic material produced by β-caryophyllene ozonolysis, *Atmos. Chem. Phys.*, *11*, 121–132, doi:10.5194/acp-11-121-2011.

Lin, G., J. E. Penner, and C. Zhou (2016), How will SOA change in the future?, *Geophys. Res. Lett.*, *43*, 1718–1726, doi:10.1002/2015GL067137.

Lin, G., J. E. Penner, S. Sillman, D. Taraborrelli, and J. Lelieveld (2012), Global modeling of SOA formation from dicarbonyls, epoxides, organic nitrates and peroxides, *Atmos. Chem. Phys.*, *12*, 4743–4774, doi:10.5194/acp-12-4743-2012.

Liu, H., D. J. Jacob, I. Bey, R. M. Yantosca, B. N. Duncan, and G. W. Sachse (2003), Transport pathways for Asian pollution outflow over the Pacific: Interannual and seasonal variations, *J. Geophys. Res.*, *108*, 8786, doi:10.1029/2002JD003102.

Mahowald, N., D. S. Ward, S. Kloster, M. G. Flanner, C. L. Heald, N. G. Heavens, P. G. Hess, J.-F. Lamarque, and P. Y. Chuang (2011), Aerosol impacts on climate and biogeochemistry, *Annu. Rev. Env. Resour.*, *36*, 45–74, doi:10.1146/annurev-environ-042009-094507.

Mann, G. W., K. S. Carslaw, D. V. Spracklen, D. A. Ridley, P. T. Manktelow, M. P. Chipperfield, S. J. Pickering, and C. E. Johnson (2010), Description and evaluation of GLOMAP-mode: A modal global aerosol microphysics model for the UKCA composition-climate model, *Geosci. Model Dev.*, *3*, 519–551, doi:10.5194/gmd-3-519-2010.

Matsui, H., M. Koike, N. Takegawa, Y. Kondo, R. J. Griffin, Y. Miyazaki, Y. Yokouchi and T. Ohara (2009), Secondary organic aerosol formation in urban air: Temporal variations and possible contributions from unidentified hydrocarbons, *J. Geophys. Res.*, *114*, D04201, doi:10.1029/2008JD010164.

McKeen, S., et al. (2007), Evaluation of several $PM_{2.5}$ forecast models using data collected during the ICARTT/NEAQS 2004 field study, *J. Geophys. Res.*, *112*, D10S20, doi:10.1029/2006JD007608.

Nannoolal, Y., J. Rarey, D. Ramjugernath, and W. Cordes (2004), Estimation of pure component properties. Part 1. Estimation of the normal boiling point of non-electrolyte organic compounds via group contributions and group interactions, *Fluid Phase Equilib.*, *226*, 45–63, doi:10.1016/j.fluid.2004.09.001.

Nannoolal, Y., J. Rarey, and D. Ramjugernath (2008), Estimation of pure component properties. Part 3. Estimation of the vapor pressure of non-electrolyte organic compounds via group contributions and group interactions, *Fluid Phase Equilib.*, *269*, 117–133, doi:10.1016/j.fluid.2008.04.020.

Ng, N. L., J. H. Kroll, A. W. H. Chan, P. S. Chhabra, R. C. Flagan, and J. H. Seinfeld (2007), Secondary organic aerosol formation from m-xylene, toluene, and benzene, *Atmos. Chem. Phys.*, *7*, 3909–3922, doi:10.5194/acp-7-3909-2007.

Nguyen, T. L., R. Winterhalter, G. Moortgat, B. Kanawati, J. Peeters, and L. Vereecken (2009), The gas-phase ozonolysis of β-caryophyllene ($C_{15}H_{24}$). Part 2: A theoretical study, *Phys. Chem. Chem. Phys.*, *11*, 4173–4183, doi:10.1039/b817913a.

O'Donnell, D., K. Tsigaridis, and J. Feichter (2011), Estimating the direct and indirect effects of secondary organic aerosols using ECHAM5-HAM, *Atmos. Chem. Phys.*, *11*, 8635–8659, doi:10.5194/acp-11-8635-2011.

Pankow, J. F. (1994), An absorption model of gas-particle partitioning involved in the formation of secondary organic aerosol, *Atmos. Environ.*, *28*, 189–193, doi:10.1016/1352-2310(94)90094-9.

Parshintsev, J., J. Nurmi, I. Kilpeläinen, K. Hartonen, M. Kulmala, and M.-L. Riekkola (2008), Preparation of β-caryophyllene oxidation products and their determination in ambient aerosol samples, *Anal. Bioanal. Chem.*, *390*, 913–919, doi:10.1007/s00216-007-1755-4.

Paulot, F., J. D. Crounse, H. G. Kjaergaard, A. Kürten, J. M. S. Clair, J. H. Seinfeld, and P. O. Wennberg (2009), Unexpected epoxide formation in the gas-phase photooxidation of isoprene, *Science*, *325*, 730–733, doi:10.1126/science.1172910.

Pye, H. O. T., and J. H. Seinfeld (2010), A global perspective on aerosol from low-volatility organic compounds, *Atmos. Chem. Phys.*, *10*, 4377–4401, doi:10.5194/acp-10-4377-2010.

Richters, S., H. Herrmann, and T. Berndt (2015), Gas-phase rate coefficients of the reaction of ozone with four sesquiterpenes at 295 ± 2 K, *Phys. Chem. Chem. Phys.*, *17*, 11658, doi:10.1039/c4cp05542j.

Robinson, A. L., N. M. Donahue, M. K. Shrivastava, E. A. Weitkamp, A. M. Sage, A. P. Grieshop, T. E. Lane, J. R. Pierce, and S. N. Pandis (2007), Rethinking organic aerosols: Semivolatile emissions and photochemical aging, *Science*, *315*, 1259–1262, doi:10.1126/science.1133061.

Sakulyanontvittaya, T., A. Guenther, D. Helmig, J. Milford, and C. Wiedinmyer (2008), Secondary organic aerosol from sesquiterpene and monoterpene emissions in the United States, *Environ. Sci. Technol.*, *42*, 8784–8790, doi:10.1021/es800817r.

Sato, K., A. Takami, Y. Kato, T. Seta, Y. Fujitani, T. Hikida, A. Shimono, and T. Imamura (2012), AMS and LC/MS analyses of SOA from the photooxidation of benzene and 1,3,5-trimethylbenzene in the presence of NO_x: Effects of chemical structure on SOA aging, *Atmos. Chem. Phys.*, *12*, 4667–4682, doi:10.5194/acp-12-4667-2012.

Scott, C. E., et al. (2014), The direct and indirect radiative effects of biogenic secondary organic aerosol, *Atmos. Chem. Phys.*, *14*, 447–470, doi:10.5194/acp-14-447-2014.

Spracklen, D. V., B. Bonn, and K. S. Carslaw (2008), Boreal forests, aerosols and the impacts on clouds and climate, *Philos. Trans. R. Soc. A Math. Phys. Eng. Sci.*, *366*, 4613–4626.

Spracklen, D. V., et al. (2011), Aerosol mass spectrometer constraint on the global secondary organic aerosol budget, *Atmos. Chem. Phys.*, *11*, 12109–12136, doi:10.5194/acp-11-12109-2011.

Stevenson, D. S., W. J. Collins, C. E. Johnson, and R. G. Derwent (1998), Intercomparison and evaluation of atmospheric transport in a Lagrangian model (STOCHEM), and an Eulerian model (UM), using ^{222}Rn as a short-lived tracer, *Q. J. R. Meteorol. Soc.*, *124*, 2477–3492.

Tasoglou, A., and S. N. Pandis (2015), Formation and chemical aging of secondary organic aerosol during the β-caryophyllene oxidation, *Atmos. Chem. Phys.*, *15*, 6035–6046, doi:10.5194/acp-15-6035-2015.

Tsigaridis, K., and M. Kanakidou (2003), Global modelling of secondary organic aerosol in the troposphere: A sensitivity analysis, *Atmos. Chem. Phys.*, *3*, 1849–1869, doi:10.5194/acp-3-1849-2003.

Tsigaridis, K., M. Krol, F. J. Dentener, Y. Balkanski, J. Lathière, S. Metzger, D. A. Hauglustaine, and M. Kanakidou (2006), Change in global aerosol composition since preindustrial times, *Atmos. Chem. Phys.*, *6*, 5143–5162, doi:10.5194/acp-6-5143-2006.

Tsigaridis, K., and M. Kanakidou (2007), Secondary organic aerosol importance in the future atmosphere, *Atmos. Environ.*, *41*, 4682–4692, doi:10.1016/j.atmosenv.2007.03.045.

Tsigaridis, K., et al. (2014), The Aerocon evaluation and intercomparison of organic aerosol in global models, *Atmos. Chem. Phys.*, *14*, 10845–10895, doi:10.5194/acp-14-10845-2014.

Utembe, S. R., L. A. Watson, D. E. Shallcross, and M. E. Jenkin (2009), A Common Representative Intermediates (CRI) mechanism for VOC degradation. Part 3: Development of a secondary organic aerosol module, *Atmos. Environ.*, *43*, 1982–1990, doi:10.1016/j.atmosenv.2009.01.008.

Utembe, S. R., M. C. Cooke, A. T. Archibald, D. E. Shallcross, R. G. Derwent, and M. E. Jenkin (2011), Simulating secondary organic aerosol in a 3-D Lagrangian chemistry transport model using the reduced Common Representative Intermediates mechansim (CRI v2-R5), *Atmos. Environ.*, *45*, 1604–1614, doi:10.1016/j.atmosenv.2010.11.046.

van Aardenne, J., J. F. Dentener, J. G. J. Olivier, C. G. M. Klein Goldewijk, and J. Lelieveld (2001), A 1° × 1° resolution dataset of historical anthropogenic trace gas emissions for the period 1890–1990, *Global Biogeochem. Cycles*, *15*, 909–928, doi:10.1029/2000GB001265.

Volkamer, R., J. L. Jimenez, F. S. Martini, K. Dzepina, Q. Zhang, D. Salcedo, L. T. Molina, D. R. Worsnop and M. J. Molina (2006), Secondary organic aerosol formation from anthropogenic air pollution: Rapid and higher than expected, *Geophys. Res. Lett.*, *33*, L17811, doi:10.1029/2006GL026899.

Volkamer, R., F. S. Martini, L. T. Molina, D. Salcedo, J. L. Jimenez and M. J. Molina (2007), A missing sink for gas-phase glyoxal in Mexico City: Formation of secondary organic aerosol, *Geophys. Res. Lett.*, *34*, L19807, doi:10.1029/2007GL030752.

Volkamer, R., P. J. Ziemann, and M. J. Molina (2009), Secondary organic aerosol formation from acetylene (C_2H_2): Seed effect on SOA yields due to organic photochemistry in the aerosol aqueous phase, *Atmos. Chem. Phys.*, *9*, 1907–1928, doi:10.5194/acp-9-1907-2009.

Watson, L. A., D. E. Shallcross, S. R. Utembe, and M. E. Jenkin (2008), A Common Representative Intermediate (CRI) mechanism for VOC degradation. Part 2: Gas phase mechanism reduction, *Atmos. Environ.*, *42*, 7196–7204, doi:10.1016/j.atmosenv.2008.07.034.

Winterhalter, R., F. Herrmann, B. Kanawati, T. L. Nguyen, J. Peeters, L. Vereecken, and G. K. Moortgat (2009), The gas-phase ozonolysis of β-caryophyllene ($C_{15}H_{24}$). Part 1: An experimental study, *Phys. Chem. Chem. Phys.*, *11*, 4152–4172, doi:10.1039/b817824k.

Zhang, H., and Q. Ying (2011), Secondary organic aerosol formation and source apportionment in Southeast Texas, *Atmos. Environ.*, *45*, 3217–3227, doi:10.1016/j.atmosenv.2011.03.046.

Zhang, Q., et al. (2007), Ubiquity and dominance of oxygenated species in organic aerosols in anthropogenically-influenced northern hemisphere midaltitudes, *Geophys. Res. Lett.*, *34*, L13801, doi:10.1029/2007GL029979.

Zhao, Y., R. Zhang, X. Sun, M. He, H. Wang, Q. Zhang, and M. Ru (2010), Theoretical study on mechanism for O_3-initiated atmospheric oxidation reaction of β-caryophyllene, *J. Mol. Struct.: THEOCHEM*, *947*, 68–75, doi:10.1016/j.theochem.2010.01.042.